

## Absorption and Reddening in the Seyfert Galaxy NGC 3227 <sup>1</sup>

D.M. Crenshaw<sup>2</sup>, S.B. Kraemer, F.C. Bruhweiler, & J.R. Ruiz

*Catholic University of America and Laboratory for Astronomy and Solar Physics, NASA's  
Goddard Space Flight Center, Code 681, Greenbelt, MD 20771*

### ABSTRACT

We have obtained low-dispersion spectra of NGC 3227 with the Space Telescope Imaging Spectrograph (STIS) to study the intrinsic UV absorption and the reddening of the nucleus in this Seyfert 1 galaxy. The UV spectra show a wealth of absorption lines at the systemic redshift that span a wide range in ionization state (Mg I to N V). The equivalent widths of the lines are consistent with our earlier prediction that a “lukewarm absorber” ( $T_e = 18,000$  K at the ionized face) with a substantial column of gas ( $N_H = 2 \times 10^{21}$  cm<sup>-2</sup>) is present and likely responsible for the reddening of the nucleus. The lukewarm absorber is also responsible for most of the absorption in the X-rays at energies less than 1 keV, although a more highly ionized “warm absorber” is needed to account for the O VII and O VIII ionization edges. In addition, we require a small column ( $N_H = 5 \times 10^{19}$  cm<sup>-2</sup>) of cold gas to match the strengths of the neutral and singly-ionized lines in the UV spectra. NGC 3227 is the first Seyfert galaxy in which a strong link between the reddening and intrinsic UV absorption has been found. By comparing our STIS UV and optical spectra with those of the unreddened Seyfert NGC 4151, we have determined a reddening curve for the nuclear continuum source in NGC 3227 over the 1150 – 10,200 Å range. The reddening curve does not show a 2200 Å bump, and is steeper in the UV than reddening curves derived for the Galaxy, LMC, and SMC, suggesting a preponderance of small dust grains near the nucleus.

*Subject headings:* galaxies: individual (NGC 3227) – galaxies: Seyfert

---

<sup>1</sup>Based on observations made with the NASA/ESA Hubble Space Telescope. STScI is operated by the Association of Universities for Research in Astronomy, Inc. under NASA contract NAS5-26555.

<sup>2</sup>crenshaw@buckeye.gsfc.nasa.gov

## 1. Introduction

The nearby Seyfert 1.5 galaxy NGC 3227 ( $z = 0.00386$ ) has been studied extensively in most regions of the electromagnetic spectrum. The UV and optical emission lines and continuum from the active nucleus are known to be reddened by dust in the Seyfert galaxy, although the derived values show a large dispersion (Komossa & Fink 1997a). For example, Cohen (1983) determined  $E_{B-V} = 0.51$  from the narrow  $H\alpha/H\beta$  ratio, whereas Winge et al. (1995) used the total (narrow + broad)  $H\alpha/H\beta$  ratio to obtain  $E_{B-V} = 0.28$  (the Galactic reddening is only  $E_{B-V} = 0.02$ , Schlegel et al. 1998). *IUE* spectra show that the UV continuum is heavily reddened, as evidenced by the steep drop in continuum flux from the near to far UV (Courvoisier & Paltani 1992). X-ray observations of NGC 3227 with *ROSAT* and *ASCA* reveal the presence of an X-ray warm absorber, characterized by an ionization parameter (number of ionizing photons with energies  $> 1$  Ryd per hydrogen atom at the ionized face) of  $U = 2.4$  and hydrogen (H I plus H II) column density  $N_H = 3 \times 10^{21} \text{ cm}^{-2}$  (George et al. 1998). *IUE* observations suggest the presence of intrinsic UV absorption in Mg II, although these observations cannot rule out a Galactic origin (Ulrich 1988).

As pointed out by Komossa & Fink (1997a), the intrinsic neutral column of gas in the line of sight to NGC 3227 ( $N_{HI} < 3 \times 10^{20} \text{ cm}^{-2}$ , see also George et al. 1998) is not sufficient to produce the observed reddening, assuming a Galactic dust/gas ratio ( $N_{HI} = 5.2 \times 10^{21} E_{B-V} \text{ cm}^{-2}$ , Shull & van Steenberg 1985). Thus, Komossa & Fink suggest that the reddening arises in the much higher column of highly ionized gas responsible for the X-ray absorption. Similar cases for “dusty warm absorbers” have been made for the QSO IRAS 13349+2438 (Brandt, Fabian, & Pounds 1996) and the Seyfert galaxies NGC 3786 (Komossa & Fink 1997b), IRAS 17020+4544 (Leighly et al. 1997), and MCG –6–30–15 (Reynolds et al. 1997).

In a recent paper on the reddening in X-ray absorbed Seyfert 1 Galaxies (Kraemer et al. 2000, hereafter K2000), we presented an alternative to the dusty warm absorber model. In our model, the dust exists in a “lukewarm absorber” in which the hydrogen is ionized, but the columns of O VII and O VIII are negligible. The lukewarm absorber can be placed at relatively large distances ( $> 100$  pc) from the nucleus, and therefore account for not only the reddening of the continuum source and broad-line region (BLR), but the reddening of the narrow-line region (NLR) as well.

In K2000, we showed a specific model for a lukewarm absorber in NGC 3227. To constrain the model, we required 1) the distance from the continuum source to be greater than  $\sim 100$  pc, to account for the reddening of the majority of the NLR emission, and 2) the column density to be  $N_H = 2 \times 10^{21} \text{ cm}^{-2}$ , to account for the average reddening of  $E_{B-V} = 0.4$  from the literature (assuming the Galactic dust to gas ratio). The parameters of the

lukewarm absorber were then determined from a fit to the soft X-ray absorption observed by *ASCA* and *ROSAT* (see K2000 for details). The resulting model was characterized by the parameters  $U = 0.13$ ,  $n_H = 20 \text{ cm}^{-3}$ , and distance = 120 pc. Interestingly, most of the soft X-ray absorption can then be attributed to He II Lyman continuum absorption. Our lukewarm absorber model for NGC 3227 predicted large ionic columns of N V, C IV, Si IV, and Mg II, which we suggested could be tested with observations in the UV at higher sensitivity than possible with *IUE*.

As part of an ongoing investigation into the intrinsic UV absorption in Seyfert galaxies, we obtained spectra of NGC 3227 with the Space Telescope Imaging Spectrograph (STIS) on the *Hubble Space Telescope* (*HST*) under a STIS guaranteed time observations (GTO) program. Given the *HST* time available for this object (2 orbits), the UV spectrum is too faint to obtain reasonable signal-to-noise levels with the echelle gratings, so we opted for low-dispersion UV spectra through a long slit (a description of STIS and its instrumental configurations can be found in Leitherer et al. 2000). We also obtained optical spectra through the same slit to investigate the reddening of the continuum over a broad wavelength region.

## 2. Observations and Measurements

We observed the nucleus of NGC 3227 on 2000 February 8 using a  $52'' \times 0''.2$  slit and the STIS low-dispersion gratings. We show the details of the observations in Table 1. We reduced the spectra using the IDL software developed at NASA’s Goddard Space Flight Center for the STIS Instrument Definition Team. The nucleus dominates the light in the long-slit images. We extracted the nuclear spectra using a  $0''.3$  height (perpendicular to the dispersion). We then combined the reduced spectra from each grating in their regions of overlap to produce a final spectrum over the 1150 – 10,200 Å range at a spectral resolving power of  $\lambda/\Delta\lambda \approx 1000$ .

Figure 1 shows the STIS UV/optical spectrum of the nucleus in NGC 3227 and that of the Seyfert 1.5 galaxy NGC 4151 (Nelson et al. 2000), scaled by a factor of 0.15 in flux. The severe extinction in the UV spectrum of NGC 3227, compared to NGC 4151, is immediately obvious. The smooth curves in Figure 1 are spline fits to continuum regions that are free of any obvious contamination by absorption or emission lines including the “little blue bump” between 2200 and 4200 Å in the NGC 4151 spectrum, which consists of a blend of broad Fe II and Balmer recombination emission (Wills, Netzer, & Wills 1985). This feature may also be present in the NGC 3227 spectrum, but since it cannot be distinguished as a separate feature from the continuum emission, the continuum fit in this region may be considered an

upper limit.

In Figure 2, we show an expanded view of the UV spectrum of NGC 3227. In addition to the broad and narrow emission lines and the interstellar absorption lines from the Galaxy, a number of intrinsic absorption lines are present and identified. These absorption lines appear at the systemic redshift of NGC 3227 ( $z = 0.00386$  from H I 21 cm observations of the host galaxy, de Vaucouleurs et al. 1991), and span a wide range in the ionization potential needed to create these ions, from zero (O I, C I, Mg I) to 77.5 eV (N V). All of the absorption lines are unresolved at the velocity resolution of the spectra ( $\sim 300 \text{ km s}^{-1}$  FWHM).

To measure the absorption lines, we fit cubic splines to adjacent wavelength regions, which typically contain both continuum and emission-line contributions. Since the absorption lines are unresolved, the column densities cannot be determined directly from integration of optical depths (e.g., Crenshaw et al. 1999), and we must therefore rely on the equivalent widths and radial velocity centroids (relative to the systemic redshift). A few of the absorption lines that we have identified are blended with stronger lines, and we are not able to determine reliable values for these lines. For the blended C IV doublet, we were able to model the observed blend with two lines of approximately equal equivalent width. We show our absorption-line measurements in Table 2 (along with column densities from models discussed in section 4).

### 3. The Reddening Curve for NGC 3227

To determine a reddening curve from the nuclear continuum emission in NGC 3227, we assumed that 1) the intrinsic UV/optical continuum of NGC 4151 is essentially unreddened, and 2) the relative flux of NGC 4151 as a function of wavelength represents the intrinsic continuum spectrum of NGC 3227. The first assumption is based on the finding by Kriss et al. (1995) that the far-UV continuum of NGC 4151 is consistent with a power-law plus a small amount of reddening that is due solely to our Galaxy ( $E_{B-V} = 0.04$ , Burstein & Heiles 1982). The second assumption is based on evidence that the intrinsic continua of Seyfert 1 galaxies have a relatively standard shape, which is modified by the effects of dust and contributions from the host galaxy to produce the observed spectral energy distributions (Ward et al. 1987). We will explore the uncertainties associated with our assumptions later in this section.

Given our assumptions, we can determine the value of  $E(B-V) = 2.5 [\log(X_B) - \log(X_V)]$ , where  $X$  is the ratio of the continuum fit to NGC 4151 to that of NGC 3227 as a function of

wavelength (Figure 1), and is evaluated at the effective wavelengths of the B (4400 Å) and V (5500 Å) filters. Thus, we find that  $E(B-V) = 0.18$ . We can also determine the reddening curve at any wavelength, relative to V and as per convention normalized to  $E(B-V)$  (Savage & Mathis 1979):

$$\frac{E(\lambda - V)}{E(B - V)} \equiv \frac{A_\lambda - A_V}{A_B - A_V} = \frac{\log(X_\lambda) - \log(X_V)}{\log(X_B) - \log(X_V)}, \quad (1)$$

where  $A_B$ ,  $A_V$ , and  $A_\lambda$  are the extinctions in magnitudes at B, V, and an arbitrary  $\lambda$ .

Since we do not know the intrinsic continuum flux of NGC 3227 at any wavelength, we cannot determine the total extinction directly. Thus, we need to calibrate the above reddening curve to determine the actual extinction law:

$$\frac{A_\lambda}{E(B - V)} = \frac{E(\lambda - V)}{E(B - V)} + R_V, \quad (2)$$

by determining the offset  $R_V \equiv A_V/E(B-V)$ . The value of  $R_V$  for the “standard” Galactic reddening curve is 3.1 (Savage & Mathis 1979), but this value can vary among different lines of sight in the Galaxy (Cardelli, Clayton, & Mathis 1989). However, extinction laws appear to have essentially the same values at wavelengths  $\lambda > 7000$  Å (Cardelli et al. 1989). If we assume this is the case for NGC 3227, then  $R_V$  is the constant we need to add to  $E(\lambda-V)/E(B-V)$  to match the standard Galactic extinction law at long wavelengths.

Figure 3 shows extinction laws for the Galaxy, LMC, and SMC, along with the extinction law determined for NGC 3227 in the fashion described above. The shape of the extinction curve for NGC 3227 is very similar to the others over the 4000 – 10000 Å range, and we find that an offset of  $R_V = 3.2$  provides a good match to these curves; this value is very close to the standard Galactic value of  $R_V = 3.1$ .

The extinction curves in Figure 3 begin to differ strongly at  $\lambda < 4000$  Å. The standard Galactic curve (Savage & Mathis 1979; Seaton 1979) shows a strong 2200 Å bump, and the weakest (although substantial) rise to the UV. The LMC curve (Koornneef & Code 1981; Fitzpatrick 1985) shows a stronger rise to the UV and a less pronounced bump. The SMC curve shows the strongest rise to the UV (until now) and no detectable 2200 Å bump (Hutchings et al. 1982; Witt & Gordon 1999).

The extinction curve for NGC 3227 is extreme, in that it shows a steeper rise to the UV than all of the other curves. Furthermore, the extinction curve resembles that of the SMC, in that there is no 2200 Å bump. Interestingly, Pitman, Clayton, & Gordon (2000) find a similar result for higher luminosity AGN; specifically, there is no convincing evidence for a

2200 Å feature in the spectrum of any QSO. Tests show that lower continuum fits in the 2200 – 4200 Å region (assuming a substantial little blue bump, see section 2 and Figure 1) have little effect on the overall sharp rise to the far-UV. Given the reddening of  $E(B-V) = 0.18$ , we can determine the extinction of NGC 3227 at any wavelength from Figure 1: e.g.,  $A_\lambda(1200 \text{ Å}) = 5.3$ ,  $A_\lambda(2000 \text{ Å}) = 2.9$ ,  $A_\lambda(3000 \text{ Å}) = 1.2$ , and  $A_V(5500 \text{ Å}) = 0.58$ . With this extinction curve, we find that the intrinsic continuum flux of NGC 3227 at any wavelength is then 0.17 times that of NGC 4151 at the respective times of observation. Note, however, that the STIS spectrum of NGC 3227 was obtained at a relatively low continuum state (section 4.2), whereas that of NGC 4151 was obtained at a moderately high state (Crenshaw et al. 2000).

To test the uniqueness of our reddening curve for NGC 3227, we have explored possible systematic uncertainties associated with our assumptions. The assumption that NGC 4151 represents the intrinsic continuum spectrum of NGC 3227 is based on the observed similarity of UV/optical continua in Seyfert 1 galaxies (e.g., Wills, Netzer, & Wills 1985). Unfortunately, *HST* observations of other unreddened Seyfert 1 galaxies covering the full UV/optical range at high spatial resolution (to avoid galaxy contamination) are not yet available. Therefore, we use the extreme variations of NGC 4151 itself, which was monitored extensively with *IUE*. Clavel et al. (1990) find that the ratio of UV to optical continuum  $F_\lambda(1450)/F_\lambda(5000)$  varies by a factor of 3.1, with high ratios corresponding to high UV fluxes. However, Kaspi et al. (1996) find that a portion of this effect is due to a substantial galaxy contribution in the apertures used for optical observations; subtracting the stellar flux at 5000 Å leads to a ratio that varies by a factor of 2.1. Thus, if we assume an extremely high state for NGC 4151 and an extremely low state for NGC 3227, this factor would bring the reddening curve of NGC 3227 close to (but still above that) of the SMC, since the reddening curves of these two objects in Figure 3 differ by 1.0 mag (on average) in the 1200 - 2000 Å range (for  $E_{B-V} = 0.18$ ). Other systematic uncertainties will tend to steepen the reddening curve slightly. Assuming that the entire 2500 – 4000 bump in the observed spectrum (Figure 1) is due to the little blue bump leads to an artificial bump in the extinction curve that spans this region (with an amplitude of 0.3 mag), which does not resemble the narrower 2200 Å bump in the standard Galactic curve. Scattering of the radiation back into our line of sight could potentially “bluen” the continuum, and correction for this effect would steepen the reddening curve in the UV. However this effect must be small, since our extraction slit covers only a 15 pc x 22 pc region, and we have estimated the dusty gas cloud is  $\sim 100$  pc from the nucleus. Assuming a spherical shell with a covering factor of one and uniform scattering, only  $\sim 1\%$  of the UV light scattered in our direction enters the aperture. Furthermore, dust grain models show that most of the UV radiation is absorbed and re-emitted in the infrared, rather than scattered (Draine & Lee 1984). Thus, our estimate of the systematic uncertain-

ties show that we cannot rule out a reddening curve for NGC 3227 that is essentially the same as that of the SMC, although it is likely to be steeper.

The STIS spectra also provide an opportunity to determine the reddening of the emission lines from the inner NLR (within  $0''.15$  or 11 pc of the nucleus for  $H_o = 75 \text{ km s}^{-1} \text{ Mpc}^{-1}$ ) for comparison with the continuum reddening. At the temperatures and densities of the NLR, the He II  $\lambda 1640$  and  $\lambda 4686$  lines are due to recombination, and the intrinsic He II  $\lambda 1640/\lambda 4686$  ratio is  $\sim 7.2$  (Seaton 1978; Kraemer et al. 1994). We were able to deblend the narrow components of these lines from their broad counterparts, using the [O III] $\lambda 5007$  lines as a template, to determine an observed ratio of  $0.19 \pm 0.05$ . This yields  $A_\lambda(1640) - A_\lambda(4686) = 3.9 \pm 0.3$  mag for the narrow lines. By comparison, the continuum extinction curve yields  $A_\lambda(1640) - A_\lambda(4686) = 3.4$ . These values are in reasonably good agreement, and provide further evidence that the reddening of the continuum and emission lines is primarily due to material outside of the inner NLR (i.e., our lukewarm absorber). The small additional reddening experienced by the emission lines may be due to dust in the inner NLR, which has been detected in other Seyfert galaxies (e.g., NGC 1068, Kraemer & Crenshaw 2000).

Our value for  $E(B-V)$  in NGC 3227 ( $= 0.18$ ) is somewhat lower than previous estimates (section 1). However, previous estimates have assumed the standard Galactic extinction curve, which is clearly incorrect, and the  $E(B-V)$  values are therefore sensitive to the wavelengths of the reddening indicators used. Also, the use of narrow  $H\alpha/H\beta$  is complicated by the deconvolution of the narrow and broad components, and in particular, the deconvolution of narrow  $H\alpha$  and [N II]  $\lambda\lambda 6548, 6884$ , which may account for at least part of the large dispersion in  $E(B-V)$  values. (Unfortunately, we cannot obtain a narrow  $H\alpha/H\beta$  ratio from our own observations, because the spectral resolution of our own data does not allow an accurate deconvolution of the  $H\alpha$  and [N II] lines.) Finally, we note that previous reddening measurements were obtained for much larger projected regions ( $> 1''$ ), and the reddening may be somewhat aperture dependent.

## 4. The Intrinsic UV Absorption Lines

### 4.1. Properties of the Absorbers

The high-ionization absorption lines in Figure 2 show significant saturation, suggesting a large column of gas. In particular, the C IV  $\lambda\lambda 1548.2, 1550.8$  lines are blended and approach zero intensity in their troughs, despite the low resolution which decreases the observed depths of the cores of unresolved absorption lines. The N V  $\lambda\lambda 1238.8, 1242.8$  and S IV  $\lambda\lambda 1393.8, 1402.8$  absorption lines in Figure 2 also suggest a substantial column of ionized gas, in

that the longer wavelength member of each doublet is much stronger than the 1:2 ratio for unsaturated lines. Qualitatively, these lines confirm our prediction in K2000 that a lukewarm absorber is present in NGC 3227.

Low-ionization absorption lines are relatively rare in Seyfert 1 galaxies; in an *HST* survey, we found that only one of 10 objects with intrinsic C IV and N V absorption showed Mg II in absorption (Crenshaw et al. 1999). This object is NGC 4151, which shows not only low-ionization species, but absorption from fine-structure and metastable levels as well in most kinematic components (Kraemer et al. 2001, and references therein), indicating a range of moderate to high densities ( $n_e$  from  $10^2 \text{ cm}^{-3}$  to  $>10^9 \text{ cm}^{-3}$ ). For NGC 3227, the fine structure lines of O I, C II, Si II, and Fe II are not detected, indicating low densities ( $n_e < 100 \text{ cm}^{-3}$ ). Note that our original model in K2000 predicted negligible ionic columns of C I and Fe II. Our detection of these lines suggests the presence of a small column of cold gas, as discussed in subsequent sections.

The intrinsic absorption lines listed in Table 2 are near the systemic redshift of the host galaxy: the average radial velocity of all of the lines is  $+20 \pm 125 \text{ km s}^{-1}$ . Although most intrinsic absorbers in Seyfert 1 galaxies are in outflow, systems near the systemic redshift are not uncommon (Crenshaw et al. 1999). There is some evidence that the high-ionization lines are at a slightly different radial velocity than the low-ionization lines: the average radial velocity for N V, C IV, and Si IV is  $-70 \pm 55 \text{ km s}^{-1}$ , whereas the average radial velocity for the remaining, low-ionization lines is  $+125 \pm 50 \text{ km s}^{-1}$ . Future observations at higher dispersions would be helpful in identifying multiple kinematic components and confirming this velocity difference.

## 4.2. Photoionization Models of the Absorbers

We have generated photoionization models to match the observed equivalent widths of the absorption lines. The photoionization code has been described in previous publications (cf. Kraemer et al. 1994). The photoionization models are parameterized in terms of the number of ionizing photons per hydrogen atom at the ionized face of the absorber ( $U$ ), the density ( $n_H$ ), the distance from the ionizing source ( $D$ ), and the sum of the H I and H II column densities ( $N_H$ ). We assume that gas is ionized by the continuum radiation emitted by the central source in the active nucleus of NGC 3227. As discussed in K2000, we modeled the EUV to X-ray spectral energy distribution (SED) as a series of power-laws of the form  $F_\nu \propto \nu^{-\alpha}$ , with  $\alpha = 1$  below 13.6 eV,  $\alpha = 2$  over the range  $13.6 \text{ eV} \leq h\nu < 500 \text{ eV}$ , and  $\alpha = 0.6$  above 500 eV. Note that the spectral index above 500 eV matches the value derived from the best fit to the combined *ROSAT*/PSPC and *ASCA* datasets (George et al. 1998). Based

on this SED, and the assumption that NGC 3227 and NGC 4151 have similar optical-UV SEDs, we derived a luminosity in ionizing photons, from 13.6 eV to 10,000 eV, of  $\sim 1.5 \times 10^{53}$  photons  $\text{s}^{-1}$ . We assumed roughly solar element abundances (cf. Grevesse & Anders 1989), which are, by number relative to H, as follows: He = 0.1, C =  $3.4 \times 10^{-4}$ , N =  $1.2 \times 10^{-4}$ , O =  $6.8 \times 10^{-4}$ , Ne =  $1.1 \times 10^{-4}$ , Mg =  $3.3 \times 10^{-5}$ , Si =  $3.1 \times 10^{-5}$ , S =  $1.5 \times 10^{-5}$ , and Fe =  $4.0 \times 10^{-5}$ . Further, we assumed that both silicate and carbon dust grains are present in the gas, with a power-law distribution in sizes (see Mathis, Rumpl, & Nordsieck 1977). For our original lukewarm model, we assumed depletions of elements from gas phase typical of the Galactic interstellar medium (cf. Snow & Witt 1996): C, 65%; O, 50%; Si 95%; Mg 82%; and Fe 95% (K2000).

In K2000, we determined that the observed reddening and the bulk of the X-ray absorption could be explained by a single component of ionized gas (a lukewarm absorber), which covers the continuum source, broad-line region, and much of the narrow-line region. As discussed in Section 1 and K2000, we had previously fixed the total column density of the lukewarm absorber at  $N_H = 2 \times 10^{21} \text{ cm}^{-2}$ , based on the reddening derived from the Balmer decrement and the Galactic dust-to-gas ratio. From our empirical reddening curve for NGC 3227, we have determined  $E(B-V) = 0.18$ , roughly half the value we assumed in K2000. and consequently one might argue that  $N_H$  should be reduced by the same factor. However, since the reddening curve is quite different in NGC 3227 than in the Galaxy, it is unlikely that the Galactic relationship of the reddening to the total hydrogen column strictly applies. Furthermore, our success in fitting the soft X-ray absorption gives us confidence that the He II column density, and hence the  $U$  and  $N_H$  are roughly correct. Therefore, we have opted to keep the same parameters as before for the lukewarm component:  $U = 0.13$ ,  $n_H = 20 \text{ cm}^{-3}$ , and  $N_H = 2 \times 10^{21} \text{ cm}^{-2}$ . Note that the distance of the lukewarm absorber from the central source depends on the luminosity, and we derived  $D = 120 \text{ pc}$  from our original finding that the reddening-corrected luminosity of NGC 3227 derived from the 1992 spectra in Winge et al. (1995) is equal to that of NGC 4151 from Nelson et al. (2000). However, the smaller reddening derived in this paper places the luminosity of NGC 3227 at 0.59 times that of NGC 4151, which yields  $D = 92 \text{ pc}$ . Furthermore, we have assumed that the 1992 luminosity represents the time-averaged value, although the current STIS spectrum indicates that it is in a lower continuum state than in previous observations (i.e., the continuum flux at  $5500 \text{ \AA}$  is 30% that of the average value from the 1992 Winge et al. spectra).

As noted in section 4.1, the STIS spectra reveal the presence of saturated N V and C IV lines, in qualitative agreement with the predictions of the lukewarm model. However, the equivalent widths of the Si IV  $\lambda\lambda 1393, 1403$  lines are about twice those expected from our original model and a curve-of-growth that fits the C IV and N V lines (see the next subsection), which is evidence for a greater column of Si IV than we had predicted. We

suggest that this is the result of a smaller fractional depletion of silicon onto dust grains. This is not surprising, given the unique extinction law we have determined for NGC 3227. However, since we do not have an independent way to determine the elemental depletions for the constituents of the silicate grains, we have recomputed the lukewarm model using the Galactic depletions, scaled by 0.8 to account for the larger fraction of silicon in gas-phase, as follows: O, 41%; Si, 77%; Mg, 67%; and Fe, 78%. While the 2200 Å bump is generally assumed to be due to carbon-based grains, the origin of this feature is not well understood (see Duley & Seahra 1999, and references therein) and its relative strength may not be correlated with the amount of carbon depletion (Cardelli et al. 1996). Hence, we have assumed the same depletion of carbon as in K2000.

As we will demonstrate in section 4.3, the lukewarm model predicts relatively small ionic columns for most low-ionization species (and essentially no Fe II), although such lines are strong in our STIS spectra (Table 2). We attempted to increase the low ionization column densities by increasing  $N_H$ , but models that fit the observed EW’s of the Si II, Mg II, and Fe II lines underpredict those of the O I and C II lines. Furthermore, there is some evidence that the low ionization lines have a different velocity radial centroid than that of the high ionization lines (section 4.1). Hence, we have included an additional component of low ionization gas (a “cold component”). Based on the absence of fine structure lines of Si II and C II, the density of the cold component is  $< 100 \text{ cm}^{-2}$  and, consequently, cannot be closer to the source of ionizing radiation than the lukewarm gas (for example, if the two components were at the same radial distance, the cold component would still have a fairly high ionization parameter of  $U = 0.03$ ). Therefore, we have placed the cold component further from the nucleus and, as a result, it is screened by the lukewarm gas. In modeling this component, we have assumed the same abundances and depletions as the lukewarm component, and the following parameters:  $U = 0.00015$ ,  $n_H = 100 \text{ cm}^{-2}$ ,  $N_H = 5.2 \times 10^{19} \text{ cm}^{-2}$ , and  $D = 160 \text{ pc}$ . The column density was set to provide the best fit to the observed low ionization lines, as described in the next section. The resulting ionic column densities for both lukewarm and cold components are given in Table 2.

### 4.3. Comparison of Observations and Models

To demonstrate that the equivalent widths of the absorption lines are consistent with the predictions of our absorber models, we have generated Maxwellian curves of growth for different velocity widths (“b” values in  $\text{km s}^{-1}$ , see Spitzer et al. 1978), as shown in Figure 4. In this figure we overplot the absorption-line data from Table 2 (in a few cases, lines from the same ion have nearly identical values and only one line is plotted for clarity). For

each absorption line that is overplotted, the vertical position is determined by the observed equivalent width and the horizontal position is determined by the ionic column predicted by the model. For a group of lines to be consistent with a model, the lines should lie relatively near a single curve of growth representing a particular  $b$  value.

The top panel in Figure 4 shows our results for the lukewarm absorber model described in the previous section. This plot shows that the high-ionization lines (C IV, N V, and Si IV) are consistent with the ionic column densities from the lukewarm model and a  $b$  value of  $100 \pm 50 \text{ km s}^{-1}$ . Mg II also matches the curve of growth at  $b = 100 \text{ km s}^{-1}$ . However, the column densities of the low-ionization lines of C II, Si II and Mg I are underpredicted, and the lukewarm model predicts negligible columns of O I, C I, and Fe II. Thus, an additional component of relatively cold gas is required to match these lines.

The bottom panel in Figure 4 shows our result for the cold absorber model described in the previous section. Nearly all of the low-ionization lines are consistent with the ionic columns predicted by the model and  $b = 200 \pm 50 \text{ km s}^{-1}$ . However, the columns of Mg I and Mg II are overpredicted, which is exacerbated by the fact that some of the Mg II equivalent width must be attributed to the lukewarm absorber. This suggests that the depletion of Mg into dust may actually be somewhat larger than the value chosen for our models (i.e., 85% rather than the 67% we assumed), and that, in general, the relative depletion of the constituents of the dust grains differs from that in the Galactic ISM. The only low-ionization line that is severely underpredicted by this model is C I. Our underprediction of the C I column is likely the result of the unusually steep extinction curve in the far UV, which is not accounted for in our model of the lukewarm absorber. The large extinction inferred at  $\sim 1100 \text{ \AA}$  depletes photons with energies near the ionization potential of C I (11.26 eV), which would likely result in a substantial C I column within the slab (note only  $\sim 1\%$  of the C needs to be C I.)

Overall, the curves of growth in Figure 4 show that the equivalent widths of the absorption lines are consistent with our models of the lukewarm and cold absorbers in the line of sight to the nucleus. The different  $b$  values and possibly different velocity centroids for the low and high-ionization lines are further evidence for two components with different kinematics. Spectral observations of the absorption at higher dispersion, although challenging due to the low UV flux, would be helpful in providing further tests of and/or refinements to these models.

## 5. Conclusions

We have shown that there are three very different intrinsic components of gas in the line of sight to the nucleus of NGC 3227: an X-ray warm absorber ( $U = 2.4$ ,  $N_H = 3 \times 10^{21} \text{ cm}^{-2}$ ), a lukewarm absorber ( $U = 0.13$ ,  $N_H = 2 \times 10^{21} \text{ cm}^{-2}$ ), and a cold absorber ( $U = 1.5 \times 10^{-4}$ ,  $N_H = 5 \times 10^{19} \text{ cm}^{-2}$ ). The X-ray warm absorber, characterized by O VII and O VIII absorption edges, shows a variable column of highly ionized gas, as discussed in detail by George et al. (1998). The lukewarm absorber predicted by K2000 and revealed by the STIS spectra shows high-ionization lines (N V, C IV, Si IV) typical of intrinsic UV absorbers in most Seyfert 1 galaxies (Crenshaw et al. 1999). The low ionization lines in the STIS spectra are primarily due to the cold component, although our model indicates significant contributions to the observed C II, Si II, and Mg II from the lukewarm absorber. The H I column from the cold component is only  $3 \times 10^{19} \text{ cm}^{-2}$  (Table 2), which is much smaller than the intrinsic neutral column of  $\sim 3 \times 10^{20} \text{ cm}^{-2}$  derived from the soft X-ray absorption (Komossa & Fink 1997a; George et al. 1998). However, as we pointed out in K2000, most of the soft X-ray absorption can be attributed to He II Lyman continuum absorption from the lukewarm absorber, and thus previous estimates of the neutral column from X-ray studies of NGC 3227 are likely a factor of ten too large.

We find that our lukewarm absorber has sufficient column to provide the dust required to redden the continuum and emission lines in NGC 3227, assuming a Galactic dust-to-gas ratio. Furthermore, the lukewarm absorber is at a distance sufficient to account for the reddening of the NLR. Thus, we prefer the lukewarm absorber as the source of the reddening. Although a dusty warm absorber cannot be completely ruled out, the variability of the warm absorber in NGC 3227 over a time scale of two years suggests a location that is within light days of the central source (George et al. 1998), which is unsuitable for reddening the NLR. Further monitoring would be helpful in verifying the variability and establishing the location of the X-ray absorber.

We note that additional support for reddening by dust at large distances comes from spectropolarimetry of NGC 3227. Schmidt & Miller (1985) find that the continuum polarization increases from 1% to 3% going from 6000 Å to 3500 Å. Furthermore, narrow emission lines are polarized by the same or slightly smaller amounts as nearby continuum regions, suggesting scattering by aligned dust grains at the location or outside of the NLR. This confirms the suggestion by Thompson et al. (1980) that the nucleus, BLR, and NLR of NGC 3227 are covered by a polarizing dust cloud.

The extinction curve that we have derived for NGC 3227 has important implications for reddening corrections to Seyfert galaxies. For example, photoionization models of the NLR rely heavily on UV/optical lines ratios (e.g.,  $\text{Ly}\alpha/\text{H}\beta$ ,  $\text{C IV}/\text{H}\beta$ ) to determine the physical

conditions in the emitting gas (cf., Kraemer & Crenshaw 2000). However, the determination of intrinsic line ratios is very sensitive to the reddening curve, which is almost always assumed to be Galactic. For  $E_{B-V} = 0.18$  and the extinction curve for NGC 3227 in Figure 3, the application of the standard Galactic curve would result in an underestimate of the extinction at  $1200\text{\AA}$  of 3.6 mag (i.e., the corrected flux would be too small by a factor of 27.5). Note that this effect is mitigated if the He II  $\lambda 1640$  and He II  $\lambda 4686$  lines are used to determine the reddening; the long UV/optical baseline provides a crude first-order correction, even if the wrong reddening curve is assumed. However, the use of the Galactic curve would still result in substantial errors, and in particular, an overestimate of the extinction in the  $2200\text{\AA}$  bump region.

The extinction curve also has important implications for the properties of the dust near the nucleus, since the shapes of the reddening curves depend on the composition and size distribution of the dust grains. Theoretical work in this area (Mathis, Rumpl, & Nordsieck 1977; Draine & Lee 1984) attributes the ratio of UV to optical absorption to the sizes of the grains (large UV absorption corresponds to smaller average grain size). Thus, the large UV extinction suggests a smaller average size of dust grains (compared to the Galaxy) for the SMC (Pei 1992; Weingartner & Draine 2000) and, by analogy, NGC 3227. One possible explanation for the smaller grain sizes near the nucleus of this Seyfert galaxy is that they are due to shocks, which tend to destroy large grains via shattering (Jones et al. 1996).

It is interesting that NGC 4151 harbors a UV absorber with a large column but shows no evidence for dust in the gas. STIS echelle observations of NGC 4151 show a kinematic component of absorption at  $-500\text{ km s}^{-1}$  (relative to systemic) that is characterized by  $U = 0.015 - 0.060$  (variable) and  $N_H = 2.8 \times 10^{21}\text{ cm}^{-2}$  (Kraemer et al. 2001), but, as we have discussed, the UV/optical continuum of NGC 4151 shows no significant reddening. However, the high-column absorber in NGC 4151 is at a distance of only  $\sim 0.03\text{ pc}$  from the nucleus (Kraemer et al. 2001), which is the approximate dust sublimation radius for the UV luminosity of this Seyfert (Barvainis 1987). Furthermore, given the large difference in distance from the nuclear continuum source, it is possible that the high-column UV absorbers in these two Seyferts have completely different origins.

*HST* observations of the (faint) UV emission from other reddened AGN would be helpful in exploring the relationship between absorption and reddening in these objects. Given that a substantial fraction of Seyfert 1 galaxies show evidence for reddening of their continua by dust (Ward et al. 1997), it would be interesting to determine their reddening curves with the procedures we have presented in this paper. New observations would be particularly useful for determining the range of intrinsic spectrum shapes in unreddened AGN and exploring the variety of extinction laws in reddened AGN.

We thank U.J. Sofia for helpful discussions on extinction laws and depletions and L. Mag-nani for useful discussions on high-latitude galactic clouds. We thank the anonymous referee for helpful suggestions. This work was supported by NASA Guaranteed Time Observer funding to the STIS Science Team under NASA grant NAG 5-4103.

## REFERENCES

- Barvainis, R. 1987, *ApJ*, 320, 537
- Brandt, W.N., Fabian, A.C., & Pounds, K.A. 1996, *MNRAS*, 278, 326
- Cardelli, J.A., Clayton, G.C., & Mathis, J.S. 1989, *ApJ*, 345, 245
- Cardelli, J.A., Meyer, D.M., Jura, M., & Savage, B.D. 1996, *ApJ*, 467, 334
- Ckavel, J., et al. 1990, *MNRAS*, 246, 668
- Cohen, R.D. 1983, *ApJ*, 273, 489
- Courvoisier, T.J., & Paltani, S. 1992, IUE – ULDA Access Guide No. 4
- Crenshaw, D.M., Kraemer, S.B., Boggess, A., Maran, S.P., Mushotzky, R.F., & Wu, C.-C. 1999, *ApJ*, 516, 750
- Crenshaw, D.M., Kraemer, S.B., Hutchings, J.B., Danks, A.C., Gull, T.R., Kaiser, M.E., Nelson, C.H., & Weistrop, D. 2000, *ApJ*, in press
- de Vaucouleurs G., de Vaucouleurs A., Corwin H. G., Buta R. J., Paturel, G., & Fouque P. 1991, *Third Reference Catalogue of Bright Galaxies* Springer-Verlag, New York
- Draine, B.T., & Lee, H.M. 1984, *ApJ*, 285, 89
- Duley, W.W., & Seahra, S.S. 1999, *ApJ*, 522, 129
- Fitzpatrick, E.L. 1985, *ApJ*, 299, 219
- George, I.M., Mushotzky, R.F., Turner, T.J., Yaqoob, T., Ptak, A., Nandra, K., & Netzer, H. 1998, *ApJ*, 509, 146
- Grevesse, N., & Anders, E. 1989, in *Cosmic Abundances of Matter*, ed. C.J. Waddington (New York: AIP), 1
- Hutchings, J.B. 1982, *ApJ*, 255, 70
- Jones, A.P., Tielens, A.G.G.M., & Hollenbach, D.J. 1996, *ApJ*, 469, 740
- Kaspi, S., et al. 1996, *ApJ*, 470, 336
- Komossa, S., & Fink, H. 1997a, *A&A*, 327, 483

- Komossa, S., & Fink, H. 1997b, *A&A*, 327, 555
- Koornneef, J., & Code, A.D., 1981, *ApJ*, 247, 860
- Kraemer, S.B., & Crenshaw, D.M. 2000, *ApJ*, in press
- Kraemer, S.B., George, I.M., Turner, T.J., & Crenshaw, D.M. 2000, *ApJ*, 535, 53 (K2000)
- Kraemer, S.B., Wu, C.-C., Crenshaw, D.M., & Harrington, J.P. 1994, *ApJ*, 435, 171
- Kraemer, S.B., et al. 2001, *ApJ*, in press
- Kriss, B.A., et al. 1995, *ApJ*, 454, L7
- Leighly, K.M., Kay, L.E., Wills, B.J., Wills, D., & Grupe, D. 1997, *ApJ*, 489, L137
- Leitherer, C., et al. 2000, *STIS Instrument Handbook*, Version 4.1, (Baltimore: STScI).
- Mathis, J.S., Rumpl, W., & Nordsieck, K.H. 1977, *ApJ*, 217, 425
- Nelson, C.H., et al. 2000, *ApJ*, 531, 257
- Pei, Y.C. 1992, *ApJ*, 395, 130
- Pitman, K.M., Clayton, G.C., & Gordon, K.D. 2000, *PASP*, 112, 537
- Reynolds, C.S., Ward, M.J., Fabian, A.C., & Celotti, A. 1997, *MNRAS*, 291, 403
- Savage, B.D., & Mathis, J.S. 1979, *ARAA*, 17, 73
- Schlegel, D.J., Finkbeiner, D.P., & Davis, M. 1998, *ApJ*, 500, 525
- Schmidt, G.D., & Miller, J.S. 1985, *ApJ*, 290, 517
- Seaton, M.J. 1978, *MNRAS*, 185, 5P
- Seaton, M.J. 1979, *MNRAS*, 187, 73P
- Shull, J.M., & Van Steenberg, M.E. 1985, *ApJ*, 294, 599
- Snow, T.P., & Witt, A.N. 1996, *ApJ*, 468, L68
- Spitzer, L. 1978, *Physical Processes in the Interstellar Medium* (New York: John Wiley), 51
- Thompson, I., Landstreet, J.D., Stockman, H.S., Angel, J.R.P., & Beaver, E.A. 1980, *MNRAS*, 192, 53
- Ulrich, M.-H. 1988, *MNRAS*, 230, 121
- Ward, M.W., et al. 1987, *ApJ*, 315, 74
- Weingartner, J.C., & Draine, B.T. 2000, preprint
- Wills, B.J., Netzer, H., & Wills, D. 1985, *ApJ*, 288, 94
- Witt, A.N. & Gordon, K.D. 1999, *ApJ*, 528, 799

Winge, C., Peterson, B.M., Horne, K., Pogge, R.W., Pastoriza, M.G., & Storchi-Bergmann,  
T. 1995, ApJ, 445, 680

Fig. 1.— STIS UV and optical spectra of NGC 3227 and NGC 4151 (scaled in flux by a factor of 0.15). The smooth lines are spline fits to continuum regions in each spectrum.

Fig. 2.— Expanded view of the UV spectra of NGC 3227. Intrinsic absorption lines detected near the systemic redshift ( $z = 0.00386$ ) are labeled.

Fig. 3.— Reddening curve determined for NGC 3227 as a function of wavelength. Reddening curves for the Galaxy (the standard curve of Savage & Mathis 1979), LMC (Koornneef & Code 1981) and SMC (Hutchings 1982) are given for comparison.

Fig. 4.— Empirical curves of growth, based on a Maxwellian velocity distribution, for different velocity widths (“b” values given in  $\text{km s}^{-1}$ , Spitzer et al. 1978). The vertical position of each point is determined from the observed equivalent width of an absorption line. The horizontal direction is determined by the column density for the corresponding ion from the model. The upper and lower panels give values based on our models of the lukewarm and cold absorption components, respectively.

Table 1. STIS Observations of NGC 3227

| Grating | Exp. Time<br>(sec) | Coverage<br>(Å) |
|---------|--------------------|-----------------|
| G140L   | 2132               | 1150 – 1715     |
| G230L   | 1612               | 1573 – 3157     |
| G430L   | 120                | 2900 – 5710     |
| G750L   | 120                | 5267 – 10,261   |

Table 2. Intrinsic Absorption – Measurements and Models

| Line                         | $v_r^a$<br>(km s <sup>-1</sup> ) | EW <sup>b</sup><br>(Å) | N (Lukewarm) <sup>c,d</sup><br>(cm <sup>-2</sup> ) | N (Cold) <sup>c,e</sup><br>(cm <sup>-2</sup> ) | Comments on<br>Observations     |
|------------------------------|----------------------------------|------------------------|----------------------------------------------------|------------------------------------------------|---------------------------------|
| Si III $\lambda$ 1206.5      |                                  |                        | 6.8 x 10 <sup>14</sup>                             | 9.4 x 10 <sup>12</sup>                         | blended with Ly $\alpha$        |
| Ly $\alpha$ $\lambda$ 1215.7 |                                  |                        | 1.8 x 10 <sup>18</sup>                             | 3.0 x 10 <sup>19</sup>                         | saturated                       |
| N V $\lambda$ 1238.8         | -44                              | 1.46 $\pm$ 0.24        | 4.8 x 10 <sup>16</sup>                             | —————                                          |                                 |
| N V $\lambda$ 1242.8         | -71                              | 1.23 $\pm$ 0.15        | 4.8 x 10 <sup>16</sup>                             | —————                                          |                                 |
| Si II $\lambda$ 1260.4       | +103                             | 1.78 $\pm$ 0.23        | 7.7 x 10 <sup>13</sup>                             | 3.5 x 10 <sup>14</sup>                         |                                 |
| C I $\lambda$ 1277.2         | +145                             | 1.07 $\pm$ 0.39        | —————                                              | 3.4 x 10 <sup>13</sup>                         |                                 |
| O I $\lambda$ 1302.2         | -236                             | 2.94 $\pm$ 0.52        | 1.1 x 10 <sup>13</sup>                             | 1.3 x 10 <sup>16</sup>                         | includes Si II $\lambda$ 1304.4 |
| Si II $\lambda$ 1304.4       |                                  |                        | 7.7 x 10 <sup>13</sup>                             | 3.5 x 10 <sup>14</sup>                         | blended with O I                |
| C I $\lambda$ 1328.8         | +174                             | 0.99 $\pm$ 0.23        | —————                                              | 3.4 x 10 <sup>13</sup>                         | includes Gal. C II              |
| C II $\lambda$ 1334.5        | +100                             | 3.22 $\pm$ 0.24        | 1.5 x 10 <sup>15</sup>                             | 5.8 x 10 <sup>15</sup>                         |                                 |
| Si IV $\lambda$ 1393.8       | -38                              | 1.92 $\pm$ 0.45        | 1.1 x 10 <sup>15</sup>                             | —————                                          |                                 |
| Si IV $\lambda$ 1402.8       | -46                              | 1.43 $\pm$ 0.20        | 1.1 x 10 <sup>15</sup>                             | —————                                          |                                 |
| Si II $\lambda$ 1526.7       | -77                              | 1.12 $\pm$ 0.19        | 7.7 x 10 <sup>13</sup>                             | 3.5 x 10 <sup>14</sup>                         |                                 |
| C IV $\lambda$ 1548.2        | -170                             | 2.38 $\pm$ 0.24        | 7.8 x 10 <sup>16</sup>                             | —————                                          | EW from fit to doublet          |
| C IV $\lambda$ 1550.8        | -170                             | 2.38 $\pm$ 0.24        | 7.8 x 10 <sup>16</sup>                             | —————                                          | EW from fit to doublet          |
| C I $\lambda$ 1560.3         | +72                              | 1.11 $\pm$ 0.35        | —————                                              | 3.4 x 10 <sup>13</sup>                         |                                 |
| C I $\lambda$ 1656.9         | -162                             | 2.18 $\pm$ 0.34        | —————                                              | 3.4 x 10 <sup>13</sup>                         |                                 |
| Al II $\lambda$ 1670.8       | -9                               | 0.85 $\pm$ 0.23        |                                                    |                                                |                                 |
| Fe II $\lambda$ 2344.2       | +198                             | 1.89 $\pm$ 0.27        | —————                                              | 4.0 x 10 <sup>14</sup>                         |                                 |
| Fe II $\lambda$ 2374.4       |                                  |                        | —————                                              | 4.0 x 10 <sup>14</sup>                         | blended with Gal. Fe II         |
| Fe II $\lambda$ 2382.8       | +151                             | 2.40 $\pm$ 0.41        | —————                                              | 4.0 x 10 <sup>14</sup>                         |                                 |
| Fe II $\lambda$ 2586.6       |                                  |                        | —————                                              | 4.0 x 10 <sup>14</sup>                         | blended with Gal. Fe II         |
| Fe II $\lambda$ 2600.2       | +122                             | 2.24 $\pm$ 0.38        | —————                                              | 4.0 x 10 <sup>14</sup>                         |                                 |
| Mg II $\lambda$ 2796.3       | +11                              | 2.66 $\pm$ 0.32        | 1.4 x 10 <sup>14</sup>                             | 3.2 x 10 <sup>14</sup>                         |                                 |
| Mg II $\lambda$ 2803.5       | +115                             | 1.52 $\pm$ 0.20        | 1.4 x 10 <sup>14</sup>                             | 3.2 x 10 <sup>14</sup>                         |                                 |
| Mg I $\lambda$ 2853.0        | +61                              | 0.62 $\pm$ 0.11        | 2.5 x 10 <sup>12</sup>                             | 1.1 x 10 <sup>13</sup>                         |                                 |

<sup>a</sup>relative to the systemic redshift of 0.00386

<sup>b</sup>blank entry: blended with another line.

<sup>c</sup>blank entry: not predicted by model. — entry: negligible ionic column

<sup>d</sup>U = 0.13, N(H I + H II) = 2 x 10<sup>21</sup> cm<sup>-2</sup>.

<sup>e</sup>U = 1.5 x 10<sup>-4</sup>, N(H I + H II) = 5.2 x 10<sup>19</sup> cm<sup>-2</sup>.

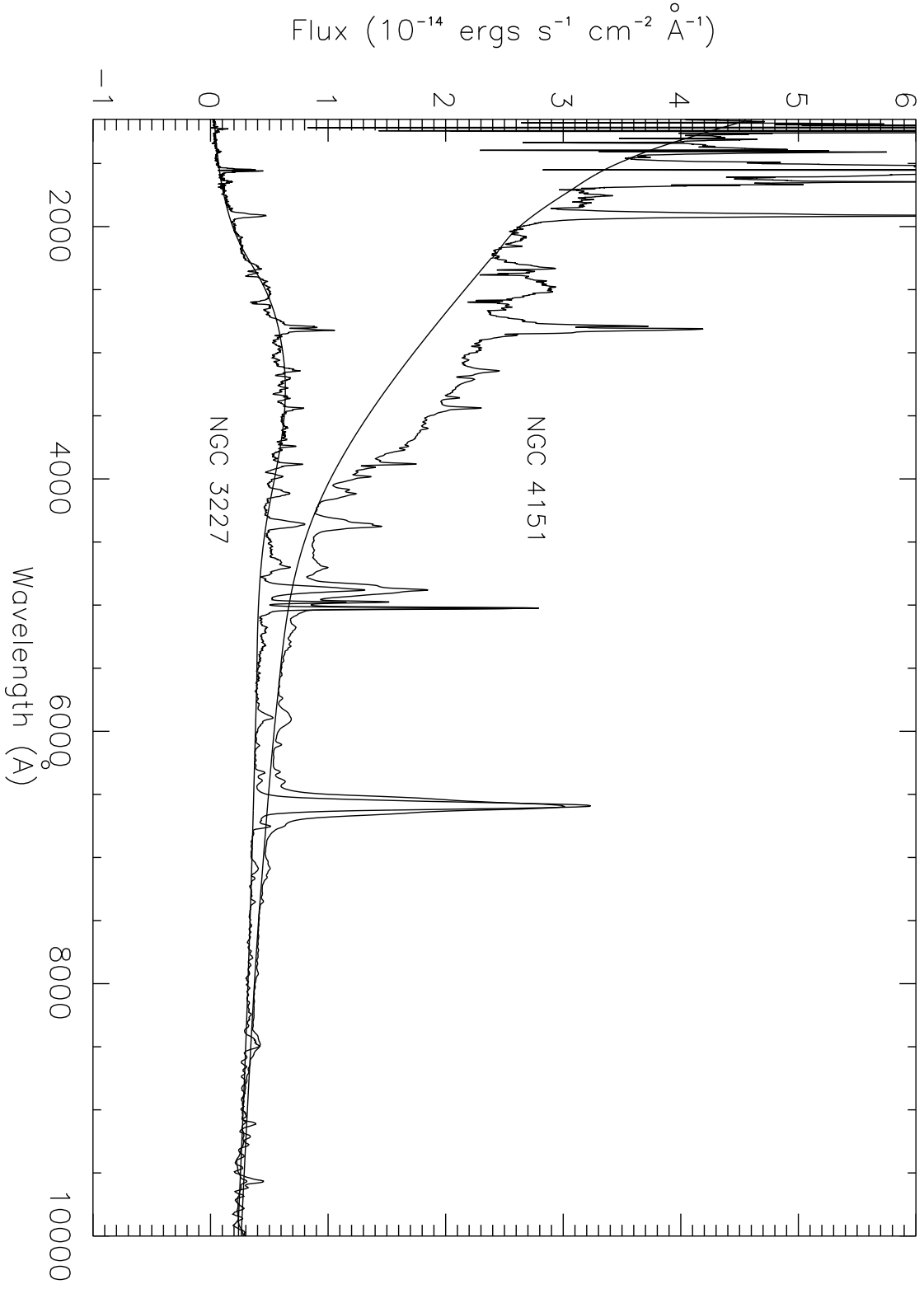


Fig. 1.

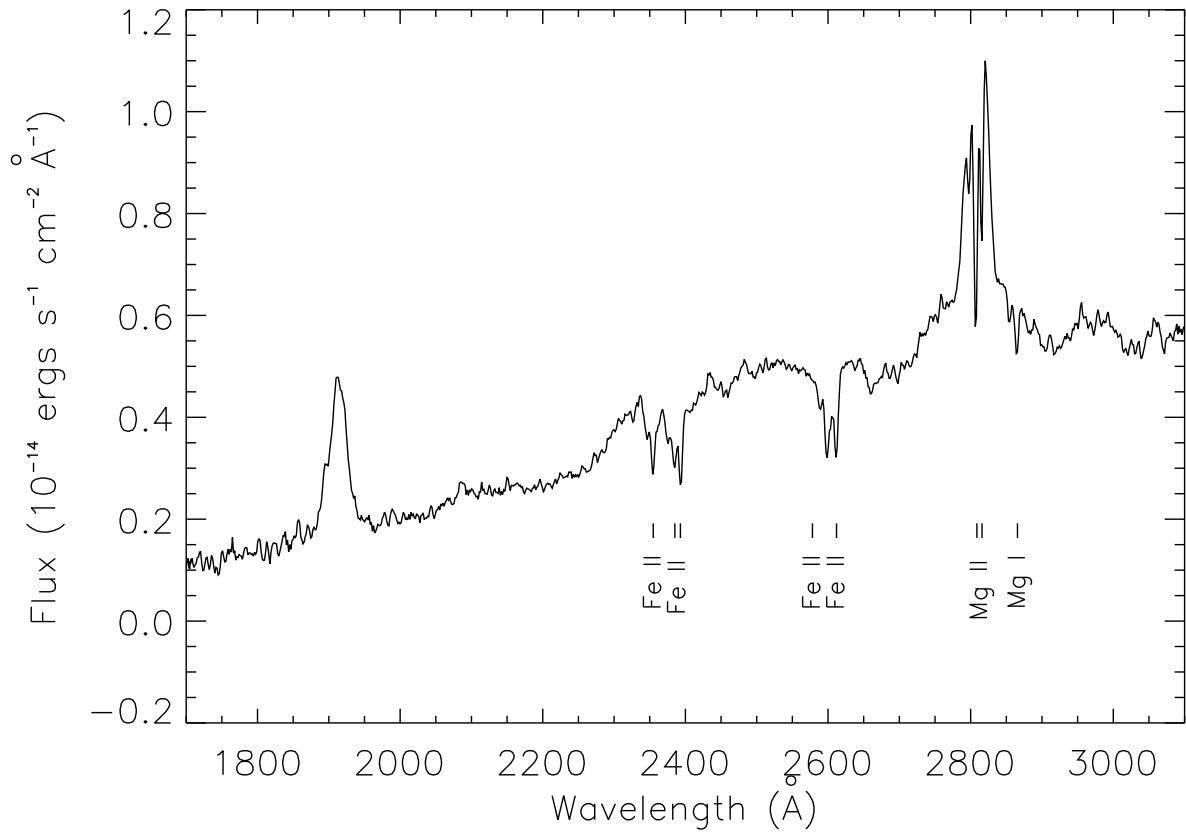
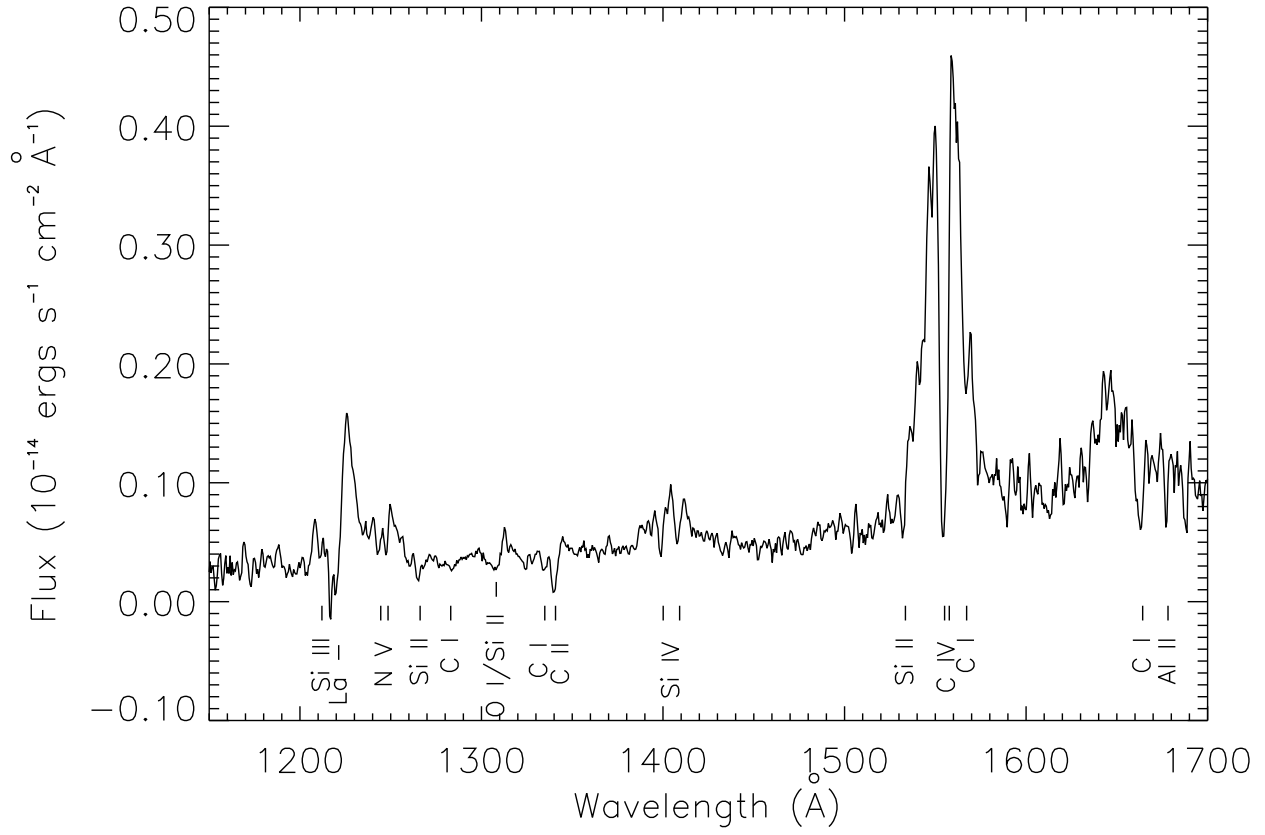


Fig. 2.

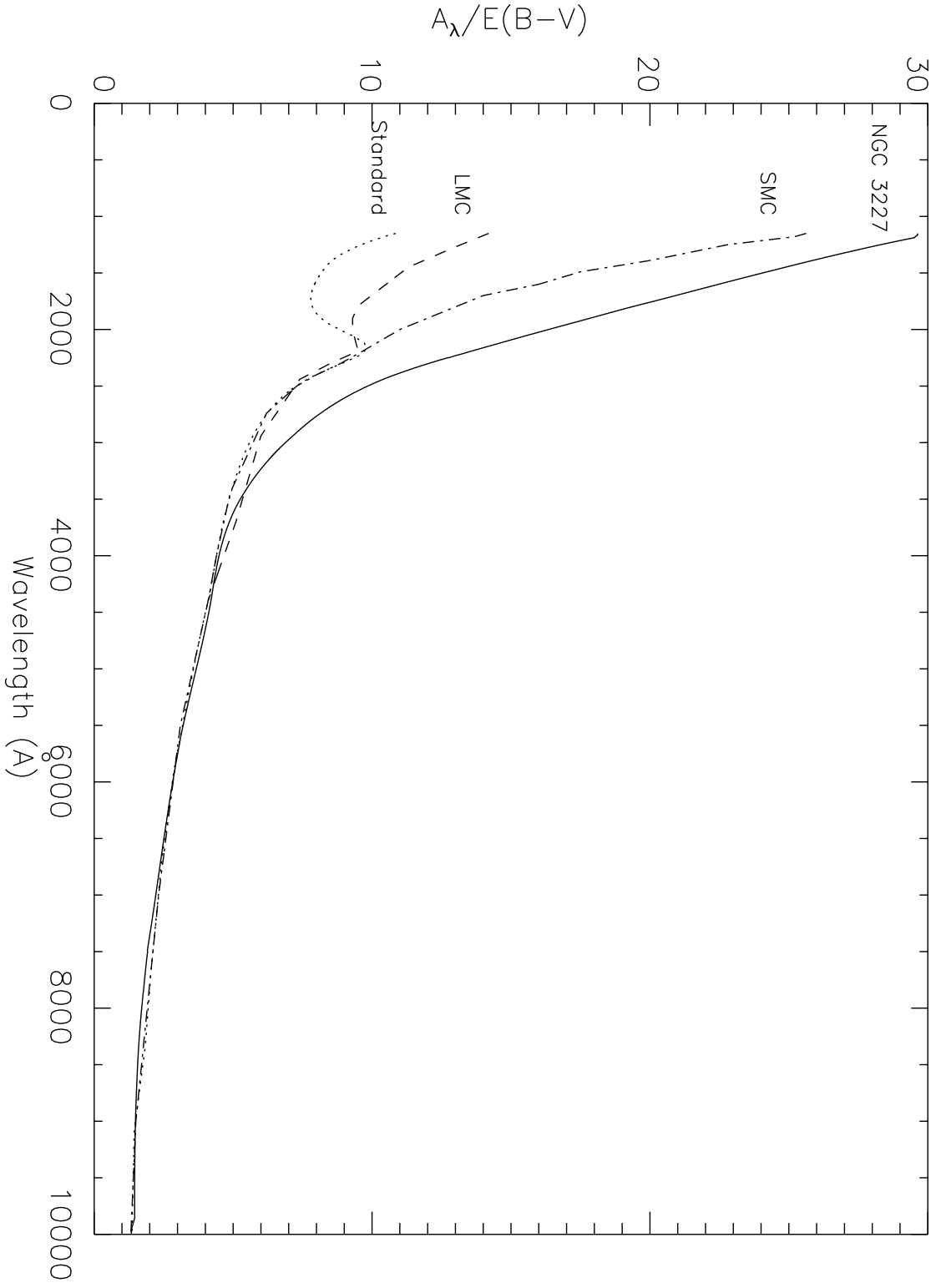


Fig. 3.

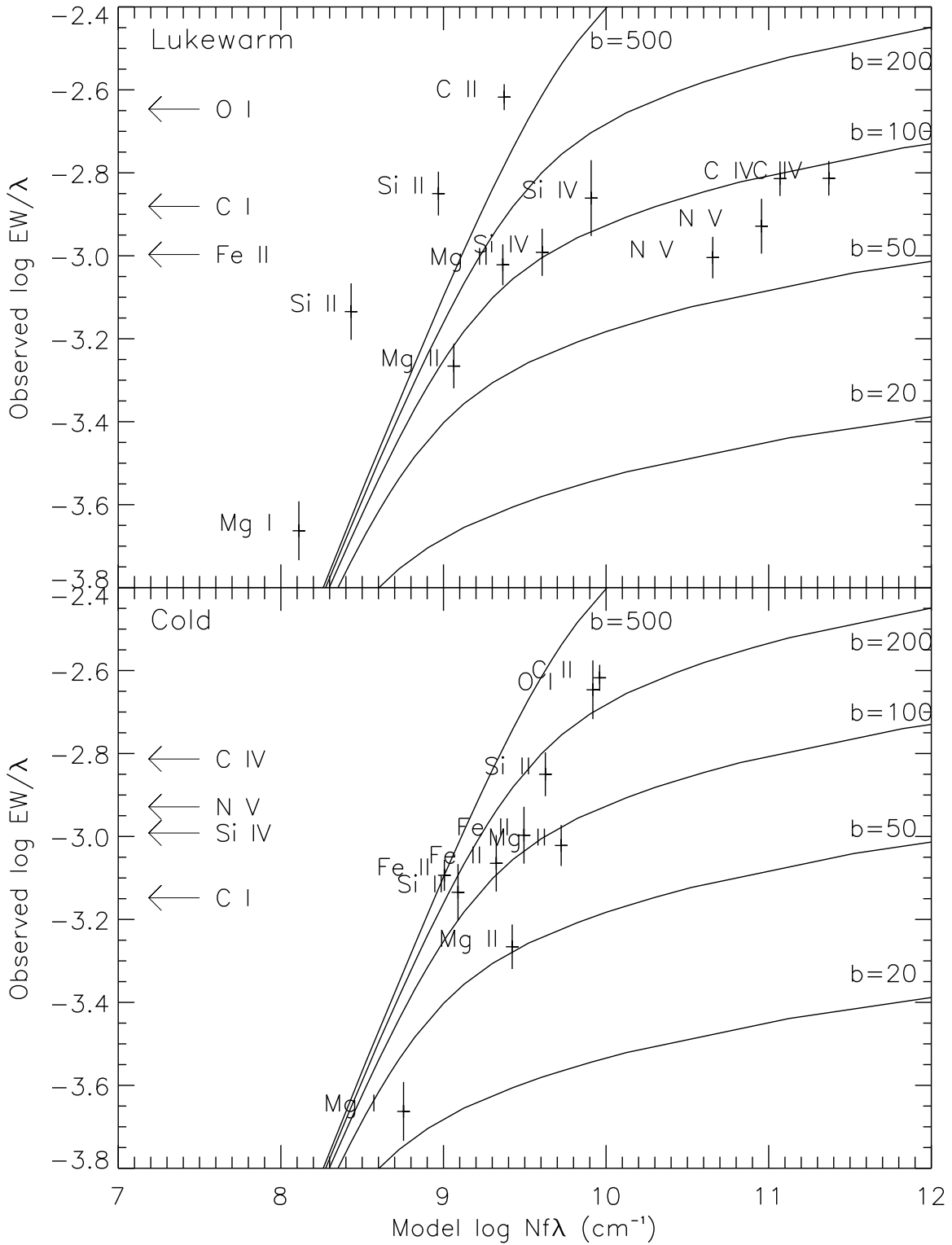


Fig. 4.